Research paper

Uniaxial compression test and numerical simulation of rock-like specimen with T-Shaped cracks

Xiong Liangxiao[1], Haijun Chen[2], Zhongyuan Xu[3], Deye Hu[4]

Abstract: In this study, the uniaxial compression test and PFC^{2D} numerical simulation were carried out on the artificial rock specimen with T-shaped prefabricated fractures. The effects of the lengths l_1, l_2 of the main fractures, the length l_3 of the secondary fracture, and the angle β between the secondary fracture and the loading direction on the uniaxial compressive strength and crack evolution law of specimen were studied. The research results show that the change of l_1, l_2 and β has obvious effect on the compressive strength and crack growth of the specimen, but the change of l_3 has little effect on the compressive strength of the specimen. When $l_3 = 40$ mm and $l_1 \neq l_2$, the angle β influences on the crack propagation and failure mode of the specimen.

Keywords: artificial rock specimen, T-Shaped crack, Uniaxial compression test

---

[1]Associate Prof., PhD., Eng., School of Civil Engineering and Architecture, East China Jiaotong University, Nanchang 330013, China, e-mail: xionglx1982@126.com, ORCID: 0000-0002-6366-5187

[2]Prof., PhD., Eng., Geotechnical Engineering Department, Nanjing Hydraulic Research Institute, Nanjing, 210029, China, e-mail: hjchen@nhri.cn, ORCID: 0000-0003-0094-9649

[3]PhD, Faculty of Geosciences and Environmental Engineering, Southwest Jiaotong University, Chengdu 611756, China, e-mail: zyxu@swjtu.edu.cn, ORCID: 0000-0003-4303-1870

[4]B.Eng., School of Civil Engineering and Architecture, East China Jiaotong University, Nanchang 330013, China, e-mail: 2573713909@qq.com, ORCID: 0000-0001-8132-0812

1. Introduction

Fractures such as faults and joints in natural rock mass have a great influence on mechanical properties and engineering stability of rock mass. Therefore, it is of great practical significance to carry out the research on the influence of fissure form on the strength characteristics and failure mode of rock. At present, many researchers conduct mechanical property test and numerical simulation on rock specimens and rock-like specimens containing crack, and it is common for specimen containing two cracks.

Huang et al. [1] performed triaxial compression experiments on sandstone samples with two preexisting closed non-overlapping flaws, the results indicate that flaw geometry has a greater impact than the confining pressure on the deformation, strength, and failure of precracked sandstone samples. Li et al. [2] conducted a numerical study on coalescence of two pre-existing parallel open flaws in rock subjected to a uniaxial compressive loading, and the numerical simulation results reveal that most of the coalescence cracks initiate at or around the flaw tips. Zhang et al. [3] performed numerical study on cracking and coalescence behavior in a rectangular rock-like specimen containing two parallel (stepped and coplanar) pre-existing open flaws under uniaxial compression load. They found that the flaw inclination angle, the ligament length and the bridging angle have different effects on the coalescence patterns, coalescence stresses as well as peak strength of specimens. Zhao et al. [4] carried out a series of uniaxial compression tests on rock-like specimens containing two flaws, and four different types of cracks and seven patterns of crack coalescences are observed in the experiments. Yang et al. [5] conducted uniaxial compression experiments on rectangular prismatic specimens of brittle sandstone containing two non-coplanar fissures, the results show that the peak strength of sandstone containing two non-coplanar fissures depends on the ligament angle, but the elastic modulus is not closely related to the ligament angle. Yang [6] carried out uniaxial compression tests for brittle sandstone samples containing two coplanar fissures, and they found that the peak strength and peak axial strain of sandstone samples containing two coplanar fissures are all lower than that of intact sample. Yao et al. [7] conducted uniaxial and triaxial compressive experiments on intact and single and double-flawed granite specimens, and found that the deformation with different numbers of flawed granite shows local gradual evolution phenomenon. Xiong et al. [8] designed uniaxial compression tests and numerical simulations on artificial jointed rock specimens with two parallel equal-length joint fractures. The results display the uniaxial compressive strength of the specimen gradually increasing with the inclination of the joint fracture with unchanged joint fracture length, rock bridge length, and the rock bridge inclination. Yang et al. [9] used the uniaxial compression test and the numerical simulation of the two-dimensional particle flow code to study the mechanical properties and failure law of rock-like specimen with parallel cracks. Their simulations indicate that the uniaxial compressive strength of the rock-like specimen with parallel cracks decreases with increasing crack length under different bridge angles. Sagong and Bobet [10] prepared and tested a number of specimens made of gypsum with three and 16 flaws in compression, and the comparisons indicate that the cracking pattern observed in specimens with multiple flaws is analogous to the pattern obtained in specimens with two

flaws. WONG and Chau [11] investigated the pattern of crack coalescence and strength of a sandstone-like material containing two parallel inclined frictional cracks under uniaxial compression, and three main modes of crack coalescence were observed. Bobet and Einstein [12] investigated fracture coalescence by loading pre-fractured specimens of gypsum used as a rock model material in uniaxial and biaxial compression. Kulatilake et al. [13] performed Laboratory experiments and numerical simulations to study the behavior of jointed blocks of model material under uniaxial loading, and investigated the effect of joint geometry parameters on the uniaxial compressive strength of jointed blocks.

The above researchers [1–13] mainly conducted mechanical test or numerical simulation on rock specimen with two parallel fractures. A few researchers carried out mechanical test and numerical simulation on rock specimens with two neither parallel nor intersecting fractures. Lee et al. [14] presented crack initiation, propagation and coalescence at or near pre-existing open cracks or flaws in a specimen under uniaxial compression, and the flaw geometry in the specimen was a combination of a horizontal flaw and an inclined flaw underneath. Yang et al. [15] performed a systematic numerical simulation to analyze the strength, deformation and fracture coalescence behavior of red sandstone containing two unparallel fissures under uniaxial compression. The results show that the peak strength and elastic modulus of red sandstone containing two unparallel fissures increase at fissure angle of 90°, before decreasing up to maximum fissure angle of 180°. Zhang et al. [16] numerically investigated crack coalescence between two non-parallel flaws in which one flaw is not underneath or is partially underneath the other and one flaw is completely underneath the other in a rock-like material. They show crack initiation and propagation leading to coalescence between the two non-parallel flaws.

There are often cross fissures in actual rock mass engineering. Xiong et al. [17] performed a series of uniaxial compression tests on artificial rock specimens feathered with cross-flaws. For jointed rock specimens with two intersecting joint planes of equal length, the uniaxial compressive strength is generally higher when the primary and the secondary joint planes are more symmetrically distributed on both sides of the loading direction. Yin et al. [18] modeled the mechanical behavior, crack initiation stress, cracking modes, and crack coalescence process experimentally due to uniaxial compressive loading for brittle granite specimens containing two orthogonal fissures, and found that mechanical parameters of granite specimens containing two orthogonal fissures are lower than the values for intact specimens. Liu et al. [19, 20] conducted a series of biaxial compression tests on rock-like precracked specimens with different cracks and confining pressures under biaxial compression, and nine crack types were observed in the experiments. However, there are few experimental results on the mechanical properties of rock specimens with cross fractures.

Therefore, the uniaxial compression test and PFC^{2D} numerical simulation were carried out on the artificial rock specimen with T-shaped prefabricated fractures. In this study, the effects of the lengths l_1, l_2 of the main fractures, the length l_3 of the secondary fracture, and the angle β between the secondary fracture and the loading direction on the uniaxial compressive strength and crack evolution law of specimen were analyzed.

2. Test principle

2.1. Specimen preparation

The size of the specimen is 100 mm × 100 mm × 100 mm. The prefabricated cracks are formed by plastic pieces, the thickness of the plastic pieces is 1 mm, and the length of the plastic pieces is 120 mm. The specimens were made by pouring cement mortar with a water-cement ratio of 0.65 into a mold. We used Portland cement #325 and quartz sand in the tests, and the sand is medium-grade standard sand, and the particle size ranges from 0.5 mm to 1.0 mm. After the initial setting of the cement mortar for 2 hours, the plastic pieces were inserted according to the positions of the cracks in Figure 1, and after another 12 hours, the plastic pieces were pulled out to form cracks in the specimen.
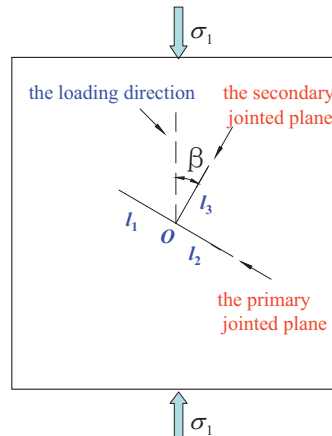
Fig. 1. Schematic diagram of uniaxial compression loading
of specimen with T-shaped fractures

Figure 1 shows the conceptualization of this experiment. The angle between the load direction and the secondary crack is defined as β, which ranges from 0° to 180°; the intersection point between the primary crack and the secondary crack is point O, and the angle between the primary crack and the secondary crack was kept at 90°; the length to the left of the point O in the main fracture is l_1, the length to the right of the point O in the main fracture is l_2, and the length of the secondary fracture is l_3; σ_1 is the vertical stress.

2.2. Test equipment

After the specimen was cured for 28 days and placed for 7 days, the specimen was placed on testing machine for uniaxial compression test. The uniaxial compression testing machine is shown in Figure 2. The loading rate was maintained at 1 kN/s during the uniaxial compression tests.

Fig. 2. Uniaxial compression testing machine

2.3. Test group

In practice, we often encounter two situations: $l_1 = l_2$ and $l_1 \neq l_2$. Therefore, the experiments were mainly grouped according to β, l_1, l_2 and l_3, and two cases of $l_1 = l_2$ and $l_1 \neq l_2$ were considered in the experiment. The test groups when $l_1 = l_2$ are shown in Table 1, and the test groups when $l_1 \neq l_2$ are shown in Table 2.

Table 1. The test groups when $l_1 = l_2$

β (°)	$l_1 = l_2$ (mm)	l_3 (mm)	Amount of specimens
0	10, 20, 30, 40	10, 20, 30, 40	48
30	40	10, 20, 30, 40	12
45	40	10, 20, 30, 40	12
60	40	10, 20, 30, 40	12
90	10, 20, 30, 40	10, 20, 30, 40	48
120	40	10, 20, 30, 40	12
135	40	10, 20, 30, 40	12
150	40	10, 20, 30, 40	12
180	10, 20, 30, 40	10, 20, 30, 40	48

The results of uniaxial compressive strength were obtained by averaging the strengths from three tested samples, which is discussed in Section 4 and Section 5. If the strength of any one specimen exceeds 15% of this averaged number, the result of this specimen is removed, and the final strength is replaced with average strength of the other two specimens.

Table 2. The test groups when $l_1 \neq l_2$

β (°)	l_1, l_2 (mm)	l_3 (mm)	Amount of specimens
0	$l_1 = 10, l_2 = 70; l_1 = 20, l_2 = 60; l_1 = 30, l_2 = 50;$ $l_1 = 50, l_2 = 30; l_1 = 60, l_2 = 20; l_1 = 70, l_2 = 10$	40	18
30	$l_1 = 10, l_2 = 70; l_1 = 20, l_2 = 60; l_1 = 30, l_2 = 50;$ $l_1 = 50, l_2 = 30; l_1 = 60, l_2 = 20; l_1 = 70, l_2 = 10$	40	18
45	$l_1 = 10, l_2 = 70; l_1 = 20, l_2 = 60; l_1 = 30, l_2 = 50;$ $l_1 = 50, l_2 = 30; l_1 = 60, l_2 = 20; l_1 = 70, l_2 = 10$	40	18
60	$l_1 = 10, l_2 = 70; l_1 = 20, l_2 = 60; l_1 = 30, l_2 = 50;$ $l_1 = 50, l_2 = 30; l_1 = 60, l_2 = 20; l_1 = 70, l_2 = 10$	40	18
90	$l_1 = 10, l_2 = 70; l_1 = 20, l_2 = 60; l_1 = 30, l_2 = 50;$ $l_1 = 50, l_2 = 30; l_1 = 60, l_2 = 20; l_1 = 70, l_2 = 10$	40	18
120	$l_1 = 10, l_2 = 70; l_1 = 20, l_2 = 60; l_1 = 30, l_2 = 50;$ $l_1 = 50, l_2 = 30; l_1 = 60, l_2 = 20; l_1 = 70, l_2 = 10$	40	18
135	$l_1 = 10, l_2 = 70; l_1 = 20, l_2 = 60; l_1 = 30, l_2 = 50;$ $l_1 = 50, l_2 = 30; l_1 = 60, l_2 = 20; l_1 = 70, l_2 = 10$	40	18
150	$l_1 = 10, l_2 = 70; l_1 = 20, l_2 = 60; l_1 = 30, l_2 = 50;$ $l_1 = 50, l_2 = 30; l_1 = 60, l_2 = 20; l_1 = 70, l_2 = 10$	40	18
180	$l_1 = 10, l_2 = 70; l_1 = 20, l_2 = 60; l_1 = 30, l_2 = 50;$ $l_1 = 50, l_2 = 30; l_1 = 60, l_2 = 20; l_1 = 70, l_2 = 10$	40	18

3. Uniaxial compression and numerical simulation of intact specimens

By simulating the uniaxial compression test of the intact specimens, reasonable meso-scopic parameters are obtained, and a numerical model consistent with the size of the test specimen is established. A square model with dimensions of 100 mm × 100 mm was established which includes 6600 circular particles of various sizes. Porosity is 0.08. The parallel bonding model is used for bonding in the PFC^{2D} simulation. In order to ensure the quasi-static loading state, the loading rate needs to be set small enough, and the axial loading rate is set as 0.05. Create servo walls around the model to prevent particles from escaping. No force is applied to the left and right walls. The T-shaped cracks are in the homogeneous and isotropic rock specimen. The particles in the PFC are treated as rigid bodies. Rigid particles are allowed to overlap at the contact point.

The numerical simulation parameters used are shown in Table 3.

The comparison result of the experimental and numerical simulated values of the uniaxial compressive stress-strain curve match well with each other (Fig. 3). Therefore, it is feasible to use the meso-parameters in Table 3.

Table 3. Numerical simulation parameters

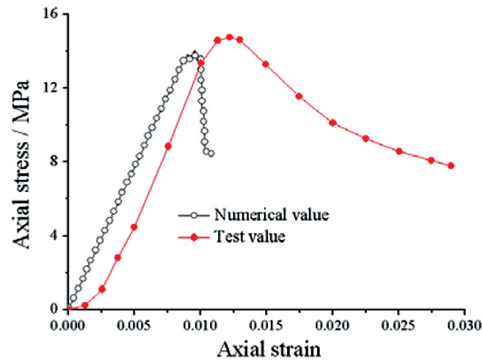| Parallel bond modulus (GPa)	Average normal bond strength (MPa)	Average tangential bond strength (MPa)	Effective modulus (GPa)	Stiffness ratio	Coefficient of friction
1.0	9.0	9.0	0.8	1.0	0.5

Fig. 3. Comparison of experimental and numerical simulation values
of stress-strain curves of intact specimen

4. Uniaxial compression and numerical simulation of specimen with T-type fractures at $l_1 = l_2$

4.1. Variation law of uniaxial compressive strength

When $l_1 = l_2 = 40$ mm and l_3 is 10 mm, 20 mm, 30 mm and 40 mm, respectively, the variation law of uniaxial compressive strength of rock mass with T-shaped fractures with β is shown in Figure 4.

When $l_1 = l_2 = 40$ mm and l_3 are fixed, the experimental value and numerical value of the uniaxial compressive strength of specimen with T-type fractures change with β as a "W" shape. The test value reaches a smaller value at β is 45° and 135°, while reaches a higher value at β is 0°, 90° and 180°. Similarly, the simulated value reaches when β is 30°, 60° and 135°, a higher value when β is 0°, 90° and 180°. Therefore, the variation law of the experimental value and the numerical value with β is basically the same.

When l_3 and β are fixed, the variation law of the test value and numerical value of the uniaxial compressive strength of specimen with T-shaped fractures with l_1 is shown in Figure 5.

When l_3 is fixed and $\beta = 0°$, the experimental value and numerical value of uniaxial compressive strength basically show a gradual decrease with l_1; when l_3 is fixed and $\beta = 90°$, the experimental value and numerical simulated value of compressive strength basically show a law of first increase and then decrease with l_1, and reach the maximum value when $l_1 = 20$ mm; when l_3 is fixed and $\beta = 180°$, the numerical value of compressive
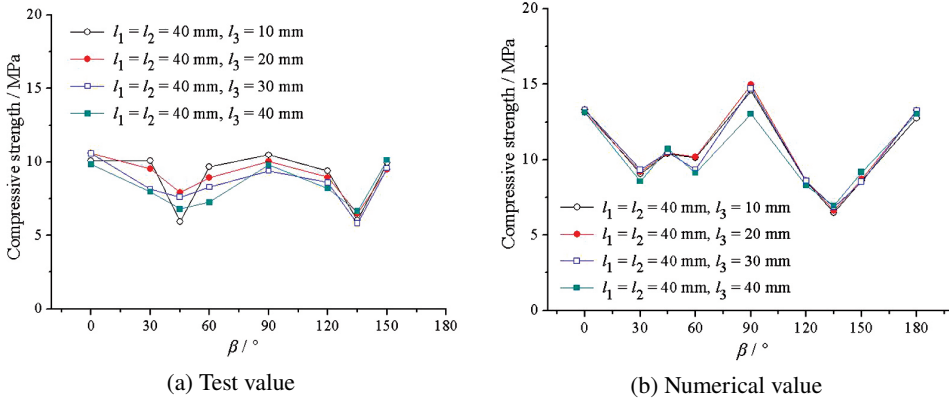
(a) Test value   (b) Numerical value

Fig. 4. The variation law of uniaxial compressive strength of specimen with T-shaped fractures with β, when $l_1 = l_2 = 40$ mm and l_3 are fixed

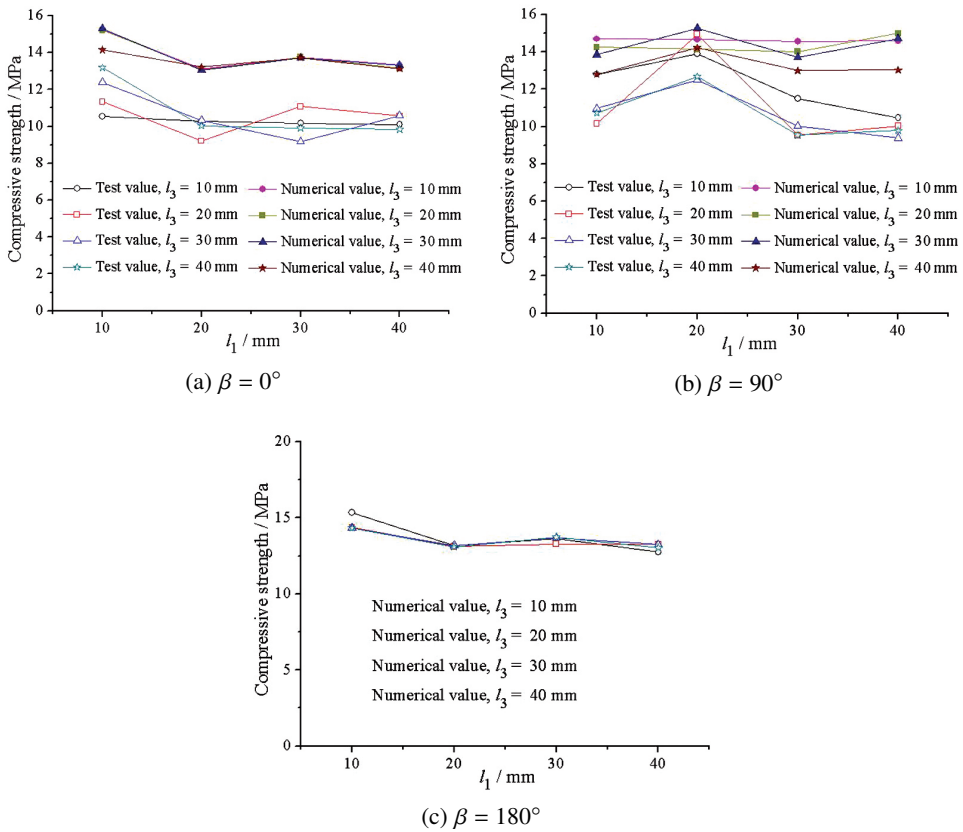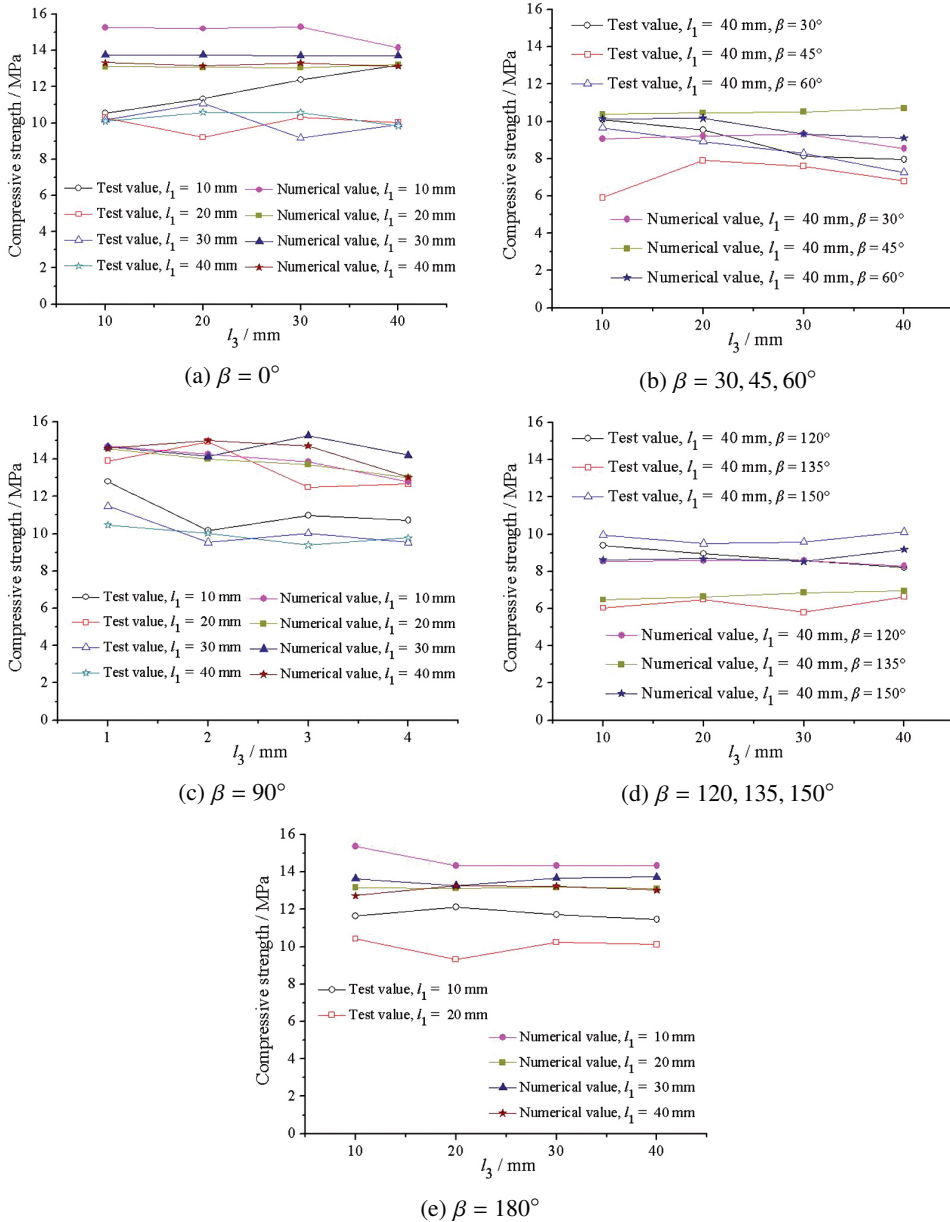(a) $\beta = 0°$ (b) $\beta = 90°$

(c) $\beta = 180°$

Fig. 5. The variation law of uniaxial compressive strength of specimen with T-shaped fractures with l_1 when l_3 and β are fixed

strength basically shows a decreasing law with l_1. The shorter the l_1 leads to a higher compressive strength since longer crack paths are needed for specimen damage.

When l_1, l_2 and β are fixed, the variation law of the experimental and simulated compressive strength with l_3 is shown in Figure 6.

(a) $\beta = 0°$

(b) $\beta = 30, 45, 60°$

(c) $\beta = 90°$

(d) $\beta = 120, 135, 150°$

(e) $\beta = 180°$

Fig. 6. The variation law of uniaxial compressive strength of specimen with T-shaped fractures with l_3 when l_1 and β are fixed

When l_1, l_2 and β remain unchanged, the change of l_3 makes the uniaxial compressive strength of the specimen fluctuate slightly around a certain value. In general, the change of l_3 has no significant effect on the uniaxial compressive strength of specimen. This conclusion obtained in this paper is also the first one obtained through experiment and numerical simulation.

4.2. The analysis of failure shape of specimen

When $l_1 = l_2 = 40$ mm, $l_3 = 10$ mm, and the test failure diagrams and numerical failure diagrams of the specimens with different β are shown in Figures 7 and 8. In Figures 7 and 8, "1" represents the prefabricated fracture, "2" represents the secondary fracture, "3" represents the tensile fracture, and "4" represents the shear fracture.

(a) $\beta = 0°$ (b) $\beta = 30°$ (c) $\beta = 45°$ (d) $\beta = 60°$ (e) $\beta = 90°$

(f) $\beta = 120°$ (g) $\beta = 135°$ (h) $\beta = 150°$ (i) $\beta = 180°$
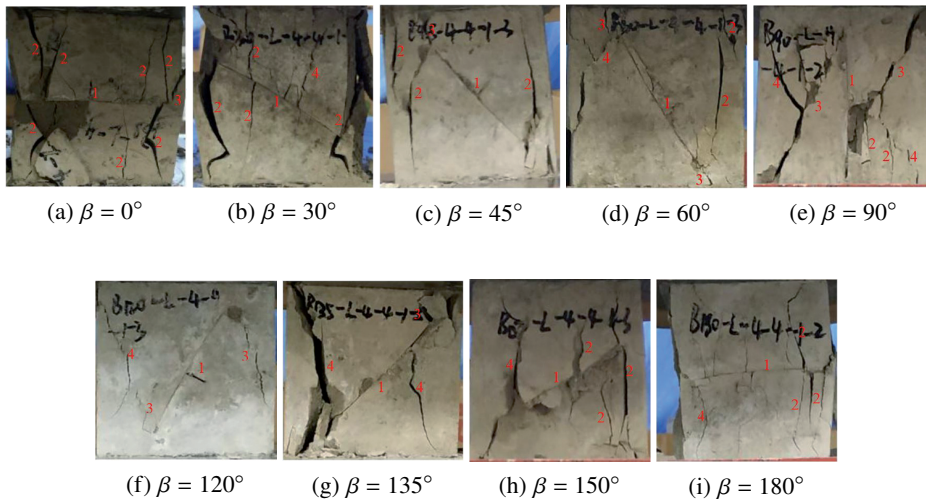
Fig. 7. The test failure diagrams of the specimen with different β when $l_1 = l_2 = 40$ mm and $l_3 = 10$ mm

When the angle β is 0° and 180°, the initial tensile cracks initiate at both ends of the main prefabricated cracks. As the loading continues, the tensile cracks expand approximately along the loading direction, and the tensile cracks penetrate through the specimen. When the angle β is 30°, 45°, 60°, 135° and 150°, not only tensile cracks but also shear cracks appear at the ends of the main prefabricated cracks. When the angle β is 30° or 45°, the specimen is damaged due to the penetration of tensile cracks; and when the angle β is 60°, 135° and 150°, the specimen is damaged due to the penetration of tensile-shear cracks. When the angle β is 90° and 120°, shear cracks generate at both ends of the main prefabricated cracks and develop along the diagonal direction of the specimen, and shear cracks or tensile-shear cracks generate at the diagonal corners of the specimen. Finally, the shear cracks penetrate the specimen and the specimen fails.

(a) $\beta = 0°$ (b) $\beta = 30°$ (c) $\beta = 45°$ (d) $\beta = 60°$ (e) $\beta = 90°$

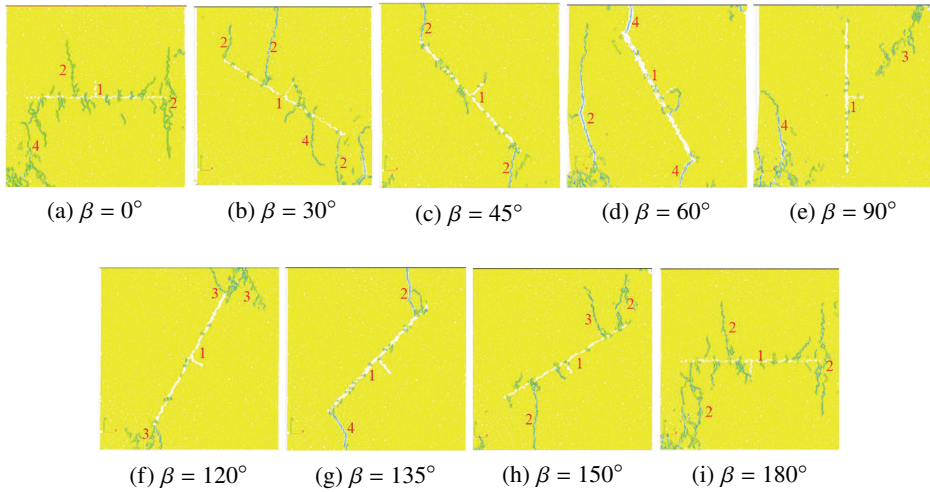(f) $\beta = 120°$ (g) $\beta = 135°$ (h) $\beta = 150°$ (i) $\beta = 180°$

Fig. 8. The numerical failure diagrams of the specimen with different β when $l_1 = l_2 = 40$ mm and $l_3 = 10$ mm

From the numerical simulation results, tensile failure appear in the specimen when the angle β is 0°, 30°, 45°, 150° and 180°, the tensile-shear failure is observed in the specimen when the angle β is 60° and 135°, and the shear failure appear in the specimen when the angle β is 90° and 120°.

Therefore, the variations of the inclined angle β of the main prefabricated crack affect the propagation of the crack and failure modes of the specimen.

When $l_3 = 40$ mm, the angle β is 90°, and the test failure diagrams and numerical failure diagrams of the specimens with different l_1 are shown in Figures 9 and 10. In Figures 9 and 10, "1" represents the prefabricated fracture, "2" represents the secondary fracture, "3" represents the tensile fracture, and "4" represents the shear fracture.

(a) $l_1 = 10$ mm   (b) $l_1 = 20$ mm   (c) $l_1 = 30$ mm   (d) $l_1 = 30$ mm
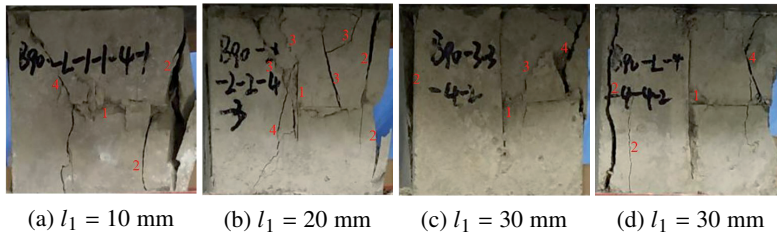
Fig. 9. The test failure diagrams of the specimen with different l_1 when $l_3 = 40$ mm and the angle β is 90°

When l_1 is 10 mm or 20 mm, shear cracks develop at both ends of the main prefabricated cracks, and overlap with the shear cracks and tensile-shear cracks at the upper and lower surfaces of the specimen to penetrate through the specimen. Tensile cracks along the
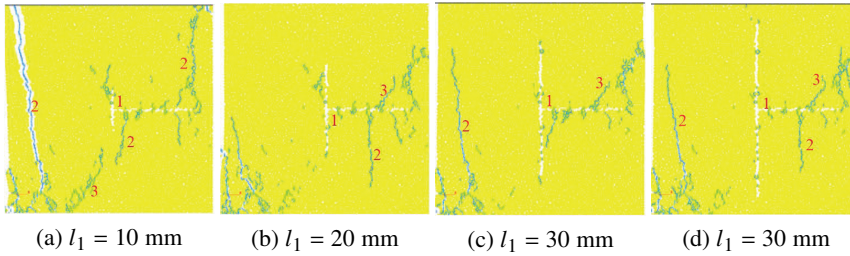
(a) l_1 = 10 mm   (b) l_1 = 20 mm   (c) l_1 = 30 mm   (d) l_1 = 30 mm

Fig. 10. The numerical simulation failure diagrams of the specimens with different l_1
when l_3 = 40 mm and the angle β is 90°

loading direction generate at the end of the secondary crack, and overlap with the tensile cracks at the upper and lower surfaces of the specimen to penetrate through the specimen. Finally, the tensile-shear failure of the specimen is caused by the combined effect of the tensile and shear cracks. When l_1 is 30 mm or 40 mm, the tensile cracks generate at the upper and lower parts and the tensile-shear cracks generate at the end of the secondary cracks. Finally, the failure of the specimen is caused by the combined effect of the tensile cracks and tensile-shear cracks.

It can be seen from the numerical simulation results that when l_1 is 10 mm, 20 mm, 30 mm and 40 mm, the tensile shear failure mainly occurs in the specimen.

Therefore, from above results, the experimental and numerical simulated results influence the expansion of cracks while has no significant effect on the failure mode of the specimen when l_1 and l_2 change at the same time.

When $l_1 = l_2 = 40$ mm, the angle β is 90°, and the test failure diagrams and numerical failure diagrams of the specimens with different l_3 are shown in Figures 11 and 12. In Figures 11 and 12, "1" represents the prefabricated fracture, "2" represents the secondary fracture, "3" represents the tensile fracture, and "4" represents the shear fracture.

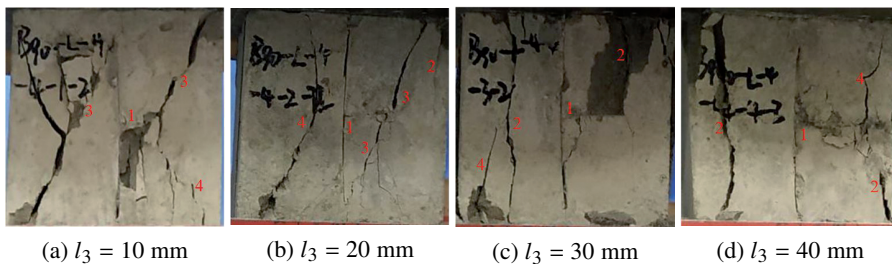(a) l_3 = 10 mm   (b) l_3 = 20 mm   (c) l_3 = 30 mm   (d) l_3 = 40 mm

Fig. 11. The test failure diagrams of the specimen with different l_3 when l_1 = 40 mm
and the angle β is 90°

When $l_3 = 10$ mm, shear cracks generate at the end of the main crack, and shear cracks and tensile-shear cracks generate at the end of secondary crack. Shear cracks generate at the upper and lower surfaces of the specimen, and expand to the prefabricated fracture, then
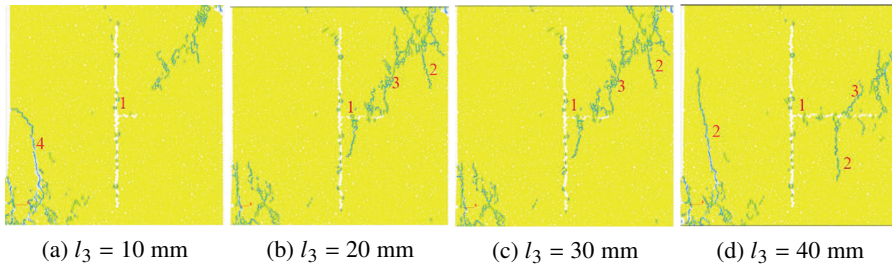
(a) $l_3 = 10$ mm   (b) $l_3 = 20$ mm   (c) $l_3 = 30$ mm   (d) $l_3 = 40$ mm

Fig. 12. The numerical failure diagrams of the specimen with different l_3 when $l_1 = 40$ mm and the angle β is $90°$

the shear cracks penetrate through the specimen, leading to the failure of the specimen. When $l_3 = 20$ mm, shear cracks generate at the ends of the main and secondary cracks, and tensile-shear cracks penetrate through the specimen which generate at the upper and lower surfaces of the specimen, and then lead to the failure of the specimen. When $l_3 = 30$ mm and 40 mm, tensile cracks and many secondary cracks occur at the ends of the secondary cracks. Tensile cracks that penetrate the specimen generate at the upper and lower surfaces of the specimen, and lead to the failure of the specimen.

It can be seen from the numerical simulation results that when $l_3 = 10$ mm or 20 mm, the numerical simulation failure of the specimen is basically consistent with the experimental failure. When $l_3 = 30$ mm, the specimen mainly suffers shear failure. When $l_3 = 40$ mm, the shear cracks generate at the end of the secondary cracks of the specimen and the tensile cracks at the upper and lower surfaces of the specimen, to the combining of them cause the failure of the specimen.

Therefore, it can be known from the experimental and numerical simulation results that when l_3 changes, it will affect the type of cracks, the mode of crack propagation and the final failure mode of the specimen.

# 5. Uniaxial compression and numerical simulation of specimen with T-type fractures when $l_1 \neq l_2$

5.1. Variation law of uniaxial compressive strength

When $l_3 = 40$ mm is fixed and $l_1 \neq l_2$, the variation law of the experimental value and numerical simulation value of the uniaxial compressive strength is shown in Figure 13.
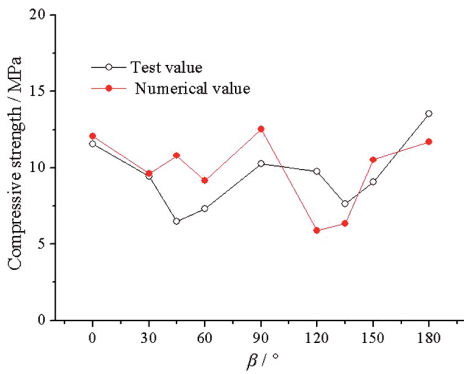
Although the test uniaxial compressive strengths and numerical simulation results of compressive strength are different, the variation behaviors of them with β are basically the same. Therefore, this difference is acceptable. When $l_1 \neq l_2$ and $l_3 = 40$ mm, both the experimental value and the numerical simulated value of the uniaxial compressive strength of rock mass with T-type fissures change with β in a W-shaped pattern. The test
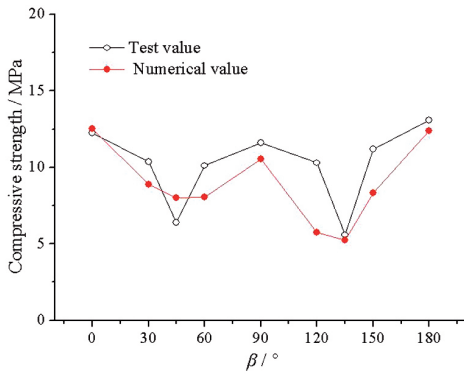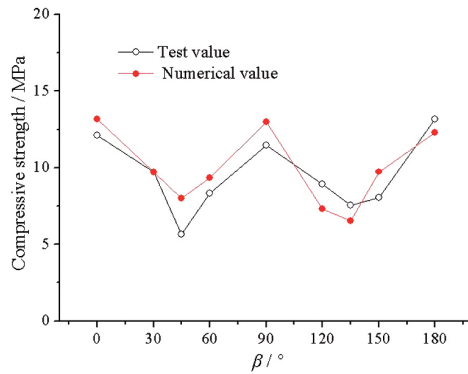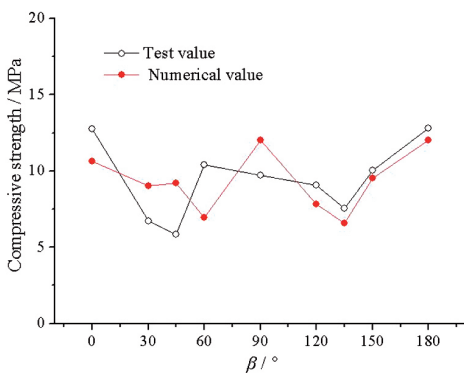
(a) $l_1 = 10$ mm, $l_2 = 70$ mm
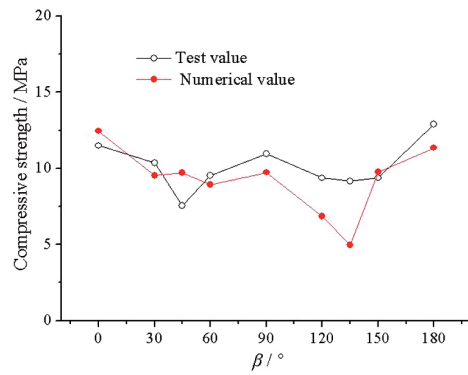
(b) $l_1 = 20$ mm, $l_2 = 60$ mm

(c) $l_1 = 30$ mm, $l_2 = 50$ mm
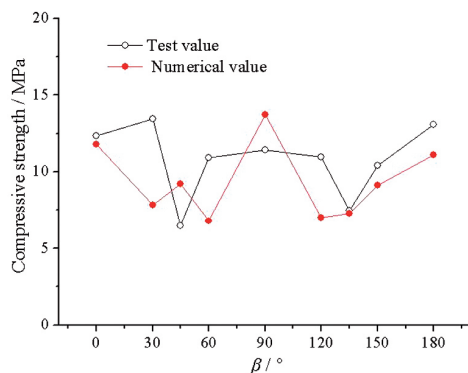
(d) $l_1 = 50$ mm, $l_2 = 30$ mm

(e) $l_1 = 60$ mm, $l_2 = 20$ mm

(f) $l_1 = 70$ mm, $l_2 = 10$ mm

Fig. 13. The variation law of uniaxial compressive strength of specimen with T-shaped fractures with β, when $l_1 \neq l_2$

value reaches a smaller value when β is 45° and 135°, and the test value reaches a larger value when β is 0°, 90° and 180°. The numerical value reaches a small value when β is 30°, 60° and 135°, and the numerical value reaches a large value when β is 0°, 90° and 180°.

5.2. Analysis of failure shape of specimen

When $l_1 = 50$ mm, $l_2 = 30$ mm, and $l_3 = 40$ mm, the test failure diagram and numerical simulation failure diagram of the specimen at different β are shown in Figures 14 and 15.

(a) $\beta = 0°$ 　　(b) $\beta = 30°$ 　　(c) $\beta = 45°$ 　　(d) $\beta = 60°$

(e) $\beta = 90°$ 　　(f) $\beta = 120°$ 　　(g) $\beta = 150°$ 　　(h) $\beta = 180°$
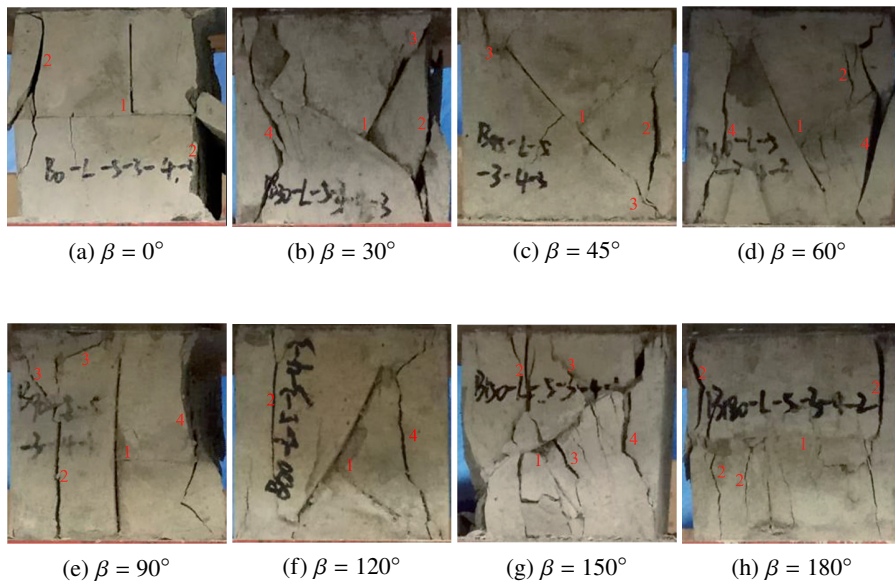
Fig. 14. The test failure diagrams of the specimen with different β
when $l_1 = 50$ mm, $l_2 = 30$ mm, $l_3 = 40$ mm

It can be seen from the test results that when β is 0° and 180°, tensile cracks develop at both ends of the main crack, and the tensile crack penetrate through the specimen and cause the specimen to failure. When β is 30°, 45°, 60°, 90°, 120°, 150° and 180°, shear cracks and tensile-shear cracks generate at the ends of the main and secondary cracks, and tensile cracks generate at the upper and lower surfaces of the specimen. Finally, the shear cracks, tensile-shear cracks and tensile cracks lead to failure of the specimen jointly. The numerical simulation failure mode of the specimen is basically consistent with the experimental failure mode. Therefore, when $l_3 = 40$ mm is fixed and $l_1 \neq l_2$, the angle β has a influence on the crack propagation and failure mode of the specimen.
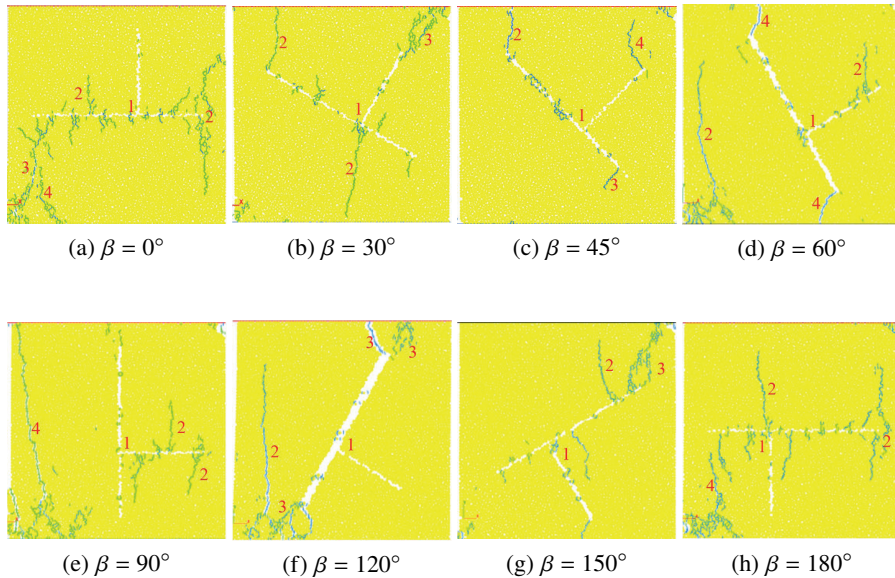
Fig. 15. The numerical failure diagrams of the specimen with different β
when $l_1 = 50$ mm, $l_2 = 30$ mm, $l_3 = 40$ mm

6. Conclusions

1. When $l_1 = l_2$ and l_3 is fixed, and $l_1 \neq l_2$ and l_3 is fixed, the variation law of experimental value and numerical simulated value of the uniaxial compressive strength are all show a "W" type. When $l_1 = l_2$, l_3 and β are fixed, the experimental value and numerical simulation value of uniaxial compressive strength basically show a gradual decreasing law with l_1 and l_2. When $l_1 = l_2$ and β are constant, the change of l_3 has limited effect on the uniaxial compressive strength of the specimen.

2. When $l_1 = l_2 = 40$ mm, $l_3 = 10$ mm, the change of the angle β of the main prefabricated cracks will affect the crack propagation and failure characteristics of the specimen. When $l_3 = 40$ mm, $l_1 = l_2$, and the angle β is 90°, the change of l_1 has some influence on the expansion of cracks, but has limited effect on the failure mode of the specimen. When $l_1 = l_2 = 40$ mm, the angle β is 90°, l_3 variations affect the type of cracks produced, the way of crack propagation and the final failure mode of the specimen. When $l_3 = 40$ mm is fixed and $l_1 \neq l_2$, the inclination angle β has an impact on the crack growth and failure mode of the specimen.

Acknowledgements

References

[1] D. Huang, D.M. Gu, C. Yang, R.Q. Huang, and G.Y. Fu, "Investigation on mechanical behaviors of sandstone with two preexisting flaws under triaxial compression", *Rock Mechanics and Rock Engineering*, vol. 49, pp. 375-399, 2016, doi: 10.1007/s00603-015-0757-3.

[2] H.Q. Li and L.N.Y. Wong, "Numerical study on coalescence of pre-existing flaw pairs in rock-like material", *Rock Mechanics and Rock Engineering*, vol. 47, pp. 2087-2105, 2014, doi: 10.1007/s00603-013-0504-6.

[3] X.P. Zhang and L.N. Y. Wong, "Crack initiation, propagation and coalescence in rock-like material containing two flaws: a numerical study based on bonded-particle model approach", *Rock Mechanics and Rock Engineering*, vol. 46, pp. 1001-1021, 2013, doi: 10.1007/s00603-012-0323-1.

[4] Y.L. Zhao, L.Y. Zhang, W.J. Wang, C.Z. Pu, W. Wan, and J.Z. Tang, "Cracking and stress–strain behavior of rock-like material containing two flaws under uniaxial compression", *Rock Mechanics and Rock Engineering*, vol. 49, pp. 2665-2687, 2016, doi: 10.1007/s00603-016-0932-1.

[5] S.Q. Yang, W.L. Tian, Y.H. Huang, P.G. Ranjith, and Y. Ju, "An experimental and numerical study on cracking behavior of brittle sandstone containing two non-coplanar fissures under uniaxial compression", *Rock Mechanics and Rock Engineering*, vol. 49, pp. 1497-1515, 2016, doi: 10.1007/s00603-015-0838-3.

[6] S.Q. Yang, "Crack coalescence behavior of brittle sandstone samples containing two coplanar fissures in the process of deformation failure", *Engineering Fracture Mechanics*, vol. 78, no. 17, pp. 3059-3081, 2011, doi: 10.1016/j.engfracmech. 2011.09.002.

[7] W. Yao, Y.Y. Cai, J. Yu, J.F. Zhou, S.Y. Liu, and B.X. Tu, "Experimental and numerical study on mechanical and cracking behaviors of flawed granite under triaxial compression", *Measurement*, vol. 145, pp. 573-582, 2019, doi: 10.1016/j.measurement.2019.03.035.

[8] L.X. Xiong, H.Y. Yuan, Y. Zhang, K.F. Zhang, and J.B. Li, "Experimental and numerical study of the uniaxial compressive stress-strain relationship of a rock mass with two parallel joints", *Archives of Civil Engineering*, vol. 65, no. 2, pp. 67-80, 2019, doi: 10.2478/ace-2019-0019.

[9] J. Yang, H.J. Chen, L.X. Xiong, Z.Y. Xu, T. Zhou, and C.H. Yang, "Analysis of uniaxial compression of rock mass with parallel cracks based on experimental study and PFC^{2D} numerical simulation", *Archives of Civil Engineering*, vol. 68, no. 1, pp. 111-128, 2022, doi: 10.24425/ace.2022.140159.

[10] M. Sagong and A. Bobet, "Coalescence of multiple flaws in a rock-model material in uniaxial compression", *International Journal of Rock Mechanics & Mining Sciences*, vol. 39, no. 2, pp. 229-241, 2002, doi: 10.1016/S1365-1609(02)00027-8.

[11] R.H.C. Wong and K.T. Chau, "Crack coalescence in a rock-like material containing two cracks", *International Journal of Rock Mechanics & Mining Sciences*, vol. 35, no. 2, pp. 147-164, 1998, doi: 10.1016/S0148-9062(97)00303-3.

[12] A. Bobet and H.H. Einstein, "Fracture coalescence in rock-type materials under uniaxial and biaxial compression", *International Journal of Rock Mechanics & Mining Sciences*, vol. 35, no. 7, pp. 863-888, 1998, doi: 10.1016/S0148-9062(98)00005-9.

[13] P.H.S.W. Kulatilake, B. Malama, and J.L. Wang, "Physical and particle flow modeling of jointed rock block behavior under uniaxial loading", *International Journal of Rock Mechanics & Mining Sciences*, vol. 38, no. 5, pp. 641-657, 2001, doi: 10.1016/S1365-1609(01)00025-9.

[14] H.W. Lee and S.W. Jeon, "An experimental and numerical study of fracture coalescence in pre-cracked specimens under uniaxial compression", *International Journal of Solids and Structures*, vol. 48, no. 6, pp. 979-999, 2011, doi: 10.1016/j.ijsolstr.2010.12.001.

[15] S.Q. Yang, Y.H. Huang, H.W. Jing, and X.R. Liu, "Discrete element modeling on fracture coalescence behavior of red sandstone containing two unparallel fissures under uniaxial compression", *Engineering Geology*, vol. 178, pp. 28-48, 2014, doi: 10.1016/j.enggeo.2014.06.005.

[16] X.P. Zhang, Q.S. Liu, S.C. Wu, and X.H. Tang, "Crack coalescence between two non-parallel flaws in rock-like material under uniaxial compression", *Engineering Geology*, vol. 199, pp. 74-90, 2015, doi: 10.1016/j.enggeo.2015.10.007.

[17] L.X. Xiong, H.J. Chen, and D.X. Geng, "Uniaxial compression study on mechanical properties of artificial rock specimens with cross-flaws", *Geotechnical and Geological Engineering*, vol. 39, pp. 1667-1681, 2021, doi: 10.1007/s10706-020-01584-z.

[18] Q. Yin, H.W. Jin, and T.T. Zhu, "Mechanical behavior and failure analysis of granite specimens containing two orthogonal fissures under uniaxial compression", *Arabian Journal of Geosciences*, vol. 9, art no. 31, 2016, doi: 10.1007/s12517-015-2078-y.

[19] X.W. Liu, Q.S. Liu, Y.S. Kang, and Y.C. Pan, "Improved nonlinear strength criterion for jointed rock masses subject to complex stress states", *International Journal of Geomechanics*, vol. 18, no. 3, 2018, doi: 10.1061/(ASCE)GM.1943-5622.0001072.

[20] X.W. Liu, Q. S. Liu, B. Liu, Y. G. Zhu, and P.L. Zhang, "Failure behavior for rocklike material with cross crack under biaxial compression", *Journal of Materials in Civil Engineering*, 2019, vol. 31, no. 2, 2019, doi: 10.1061/(ASCE)MT.1943-5533.0002540.